UC Merced
UC Merced Previously Published Works

Title
True Atomic-Resolution Surface Imaging and Manipulation under Ambient Conditions via Conductive Atomic Force Microscopy

Permalink
https://escholarship.org/uc/item/5pc5r2m2

Journal
ACS Nano, 16(12)

ISSN
1936-0851

Authors
Sumaiya, Saima A
Liu, Jun
Baykara, Mehmet Z

Publication Date
2022-12-27

DOI
10.1021/acsnano.2c08321

Peer reviewed

eScholarship.org Powered by the California Digital Library
University of California

ACS NANO

www.acsnano.org

ARTICLE

True Atomic-Resolution Surface Imaging and Manipulation under Ambient Conditions via Conductive Atomic Force Microscopy

Saima A. Sumaiya, Jun Liu, and Mehmet Z. Baykara*

Cite This: https://doi.org/10.1021/acsnano.2c08321 Read Online

ACCESS | Metrics & More | Article Recommendations | Supporting Information

ABSTRACT: **A great number of chemical and mechanical phenomena, ranging from catalysis to friction, are dictated by the atomic-scale structure and properties of material surfaces. Yet, the principal tools utilized to characterize surfaces at the atomic level rely on strict environmental conditions such as ultrahigh vacuum and low temperature. Results obtained under such well-controlled, pristine conditions bear little relevance to the great majority of processes and applications that often occur under ambient conditions. Here, we report *true* atomic-resolution surface imaging via conductive atomic force microscopy (C-AFM) under ambient conditions, performed at high scanning speeds. Our approach delivers atomic-resolution maps on a variety of material surfaces that comprise defects including single atomic vacancies. We hypothesize that atomic resolution can be enabled by either a confined, electrically conductive pathway or an individual, atomically sharp asperity at the tip−sample contact. Using our method, we report the capability of *in situ* charge state manipulation of defects on MoS_2 and the observation of an exotic electronic effect: room-temperature charge ordering in a thin transitionmetal carbide (TMC) crystal (i.e., an MXene), α-Mo_2C. Our findings demonstrate that C-AFM can be utilized as a powerful tool for atomic-resolution imaging and manipulation of surface structure and electronics under ambient conditions, with wide-ranging applicability.**

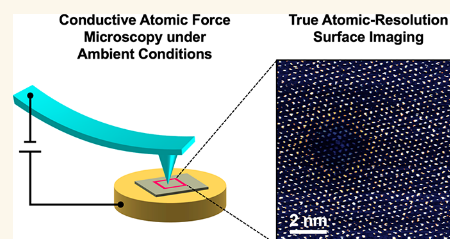

KEYWORDS: *atomic force microscopy, atomic-resolution imaging, charge ordering, defects, MXenes, two-dimensional materials*

Atomic-resolution imaging provides crucial information about the structure and physical properties of material surfaces, with implications for a multitude of fields in science and technology.[1−3] Despite this fact, direct, real-space atomic-resolution images of surfaces could not be recorded before the invention of the scanning tunneling microscope (STM) in 1982,[4] a feat that culminated in the awarding of the Nobel Prize in Physics in less than four years. The development of the atomic force microscope (AFM) in 1986 overcame the limitation of STM to conductive samples,[5] and reports of apparent atomic-resolution imaging soon followed.[6,7] It was, however, quickly discovered that such results can best be described as *lattice resolution*, as *true* atomic-resolution imaging requires the imaging of individual atomic defects such as single vacancies, which were conspicuously missing in these early works. The physical limitation that led to this failure to achieve true atomic resolution with AFM was attributed to the repulsive contact formed between the probe tip and the sample surface during *contact mode* operation. This leads to contact areas that are at least several atoms wide, resulting in an averaging of force interactions across this rather blunt interface and, consequently, the inability to image individual atomic vacancies.[8,9] On the other hand, nearly a decade after the invention of the AFM, a method named noncontact atomic force microscopy (NC-AFM) was introduced by Giessibl and then Morita's group, with which atomic-resolution imaging can be achieved on a wide range of sample surfaces by means of detecting short-range interaction forces between the sharp probe tip and the sample surface.[10,11]

A critical limitation associated with both STM and NC-AFM is that they typically cannot be performed under ambient conditions for atomic-resolution imaging. Exceptions include certain reports of atomic-resolution STM imaging under ambient conditions.[12,13] It should also be noted that great progress has been made in recording true atomic-resolution images of a wide variety of surfaces under a liquid environment, without restrictions of sample conductivity.[14,15] Finally, there has been one isolated report of true atomic-

Received: August 19, 2022
Accepted: October 21, 2022

Downloaded via F. HOFFMANN-LA ROCHE LTD on October 25, 2022 at 17:38:32 (UTC).
See https://pubs.acs.org/sharingguidelines for options on how to legitimately share published articles.

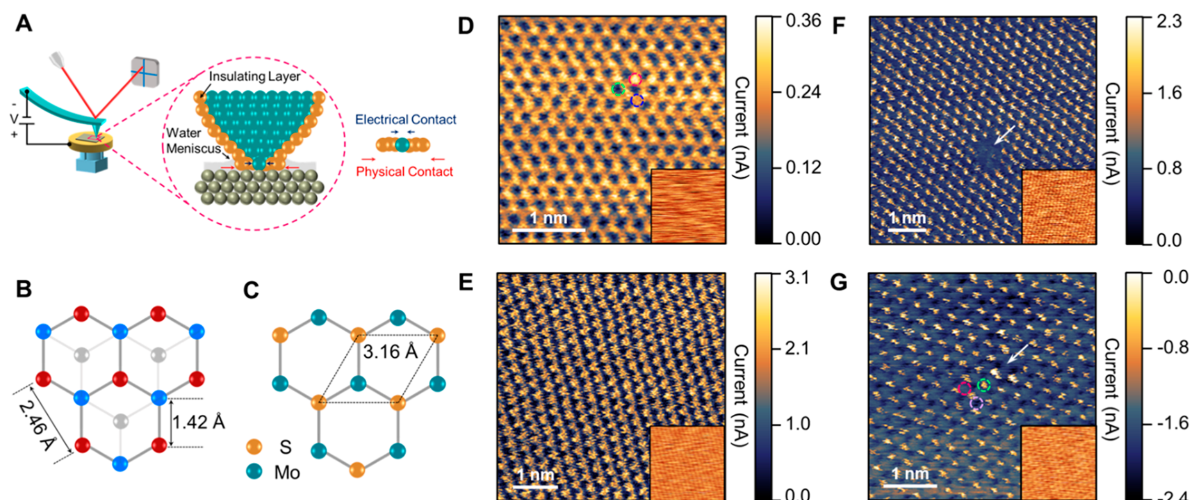

Figure 1. Demonstration of true atomic-resolution imaging under ambient conditions via C-AFM. (A) Schematic showing the C-AFM setup, along with the discrepancy between the physical and electrical contact formed between the tip and the sample, as one of the possible explanations that can enable atomic-resolution imaging. (B) Atomic model of the HOPG (0001) surface with red and blue spheres representing two types of carbon atoms, and the gray spheres representing carbon atoms in the layer below. (C) Atomic model of the MoS_2 (001) surface. (D) Current image obtained on HOPG showing three types of atomic sites characterized by low, high, and intermediate current (see the corresponding green, pink, and blue circles, respectively). The simultaneously recorded topography map (height range: 0–3.1 Å) is shown in the inset, exhibiting no atomic-scale features. (E) Current image obtained on MoS_2 showing well-defined protrusions separated by ~3.2 Å. The simultaneously obtained topography map, with a stripe-like pattern, is shown in the inset (height range: 0–6.8 Å). (F) Current image obtained on MoS_2 showing multiple atomic-scale defects. The simultaneously obtained topography map is shown in the inset, with no trace of the defects (height range: 0–3.4 Å). (G) Current image obtained on MoS_2 exhibiting three types of atomic sites characterized by low, high, and intermediate current (see the corresponding green, purple, and pink circles, respectively). This image clearly captures a single atomic defect, as indicated by the white arrow. The corresponding topography map is shown in the inset (height range: 0–5.4 Å). All images were obtained with an applied normal load of 0.0 nN and at a scanning frequency of 15.62 Hz. Bias voltages: (D) 0.04 V; (E) 0.1 V; (F) 1.8 V; (G) −1.2 V.

resolution imaging via NC-AFM on a calcite surface in air,[16] despite multiple attempts at imaging other surfaces.[17] On the other hand, in general, when they are exposed to ambient conditions, surfaces are covered with a layer of contaminants adsorbed from the environment, resulting in an insurmountable barrier to the precise detection of tunneling currents and interaction forces. In order to suppress the adsorption of contaminants and achieve atomic-resolution imaging, STM and NC-AFM are typically performed under ultrahigh-vacuum (UHV) conditions. However, adsorption/contamination in realistic environments can lead to important changes in chemical, mechanical, and electronic surface characteristics, which can have critical implications for functionality.[18,19] Moreover, processes observed under the ideal yet unrealistic UHV environment bear little relevance for technological applications such as heterogeneous catalysis, which often takes place at elevated pressures. This leads to longstanding critical issues in surface science such as the *pressure gap*.[20]

RESULTS AND DISCUSSION

A scanning probe microcopy (SPM) method that could potentially overcome the restriction of atomic-resolution STM and NC-AFM to UHV is conductive atomic force microscopy (C-AFM), whereby a conductive probe tip scans the sample surface in contact mode under the application of an electrical bias voltage, and the current flowing between the two is recorded as a function of lateral position in the form of images. Motivated by recent work that demonstrated atomic-resolution imaging on a small number of samples under controlled environmental conditions induced by a dry nitrogen atmosphere,[21,22] we performed high-speed C-AFM imaging experiments under ambient conditions (Figure 1A) on a variety of material surfaces. Our results demonstrate that true atomic-resolution imaging can be achieved via C-AFM under ambient conditions, proven by the imaging of single atomic vacancies, among other defects. Going beyond imaging, we additionally report *in situ* manipulation of defect charge states on MoS_2, as well as the observation of room-temperature change ordering on an MXene, with signatures of rotational symmetry breaking with respect to the underlying atomic lattice.

Initial measurements were first performed on the (0001) surface of highly oriented pyrolytic graphite (HOPG), a prototypical benchmark sample (see Figure 1B for the atomic model of the surface). The results are summarized by the current map in Figure 1D, where we are able to detect three types of atomic sites on the HOPG crystal characterized by low, high, and moderate current, separated by ~1.4 Å. This observation is in strong contrast to previous works in the literature that predominantly feature lattice resolution, whereby only one type of atomic site, with a periodicity of ~2.5 Å, is imaged as *bright*.[23,24] In our case, the reproducible imaging of three atomic sites separated by ~1.4 Å (which corresponds to the interatomic distance of 1.42 Å between carbon atoms that is expected on an HOPG (0001) surface) demonstrates that we are indeed able to resolve *all* carbon atoms on the HOPG surface, as well as the hollow sites that exist at the center of the hexagons formed by them.

Despite the promising result above, the key signature of true atomic-resolution imaging remains as the capability of identifying single atomic defects such as individual vacancies. We therefore turned our attention to MoS_2, a two-dimensional

https://doi.org/10.1021/acsnano.2c08321
ACS Nano XXXX, XXX, XXX−XXX

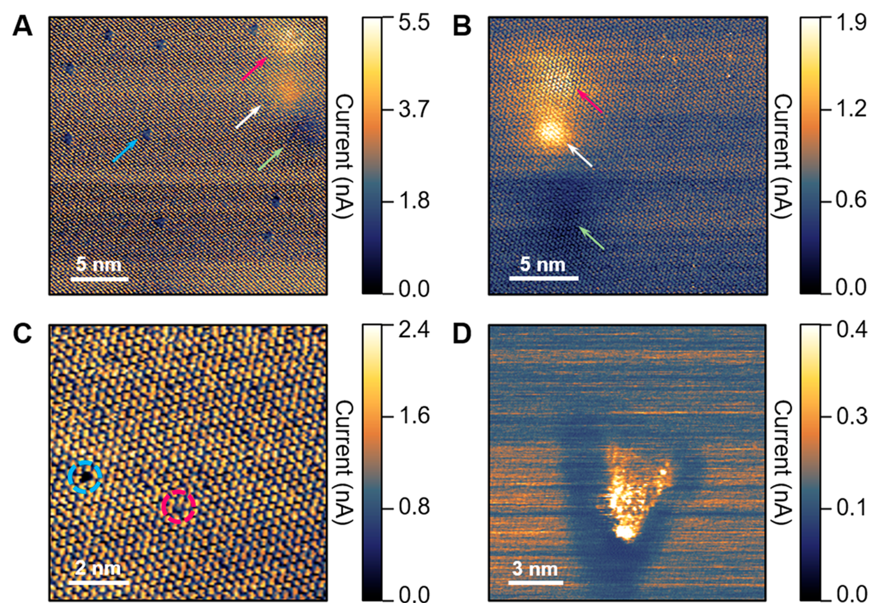

Figure 2. Imaging of different types of defects on MoS_2 (001) under ambient conditions via C-AFM. (A) Current image featuring dark, concentrated defects (blue arrow) as well as diffuse, large-area bright (pink and white arrows) and dark (green arrow) defects. (B) Enlarged current image on the diffuse defects in (A). (C) Current image exhibiting a faint, atomic-scale dark defect (pink circle) and a regular, atomic-scale dark defect (blue circle). (D) Current image showing an extended defect, with a central, bright region (enhanced conductivity) surrounded by a dark region (attenuated conductivity). All images were obtained with an applied normal load of 0.0 nN and at a scanning frequency of 15.62 Hz. Bias voltages: (A) 1.8 V; (B) 1.8 V; (C) 0.7 V; (D) 0.9 V.

(2D) semiconductor from the family of transitionmetal dichalcogenides (TMDs), which is (i) of significant electronic relevance[25] and (ii) expected to feature a higher density of defects than HOPG (see Figure 1C for an atomic model). A current map obtained on MoS_2 is shown in Figure 1E, together with the simultaneously recorded topography map in the inset. There are distinct differences between the two channels: while we observe clearly resolved, individual protrusions (separated by ∼3.2 Å, the distance between individual S as well as Mo atoms on MoS_2) in the current map, the topography map comprises vaguely resolved stripes of 0.2−0.6 Å in height. The observation of a much sharper contrast in the current channel in comparison with the topographic one indicates that the mechanism that results in high resolution in the current map is fundamentally different from that responsible for atomic-scale stick−slip patterns in the topography image.[23] On the other hand, the absence of any defects in the current map precludes us from claiming true atomic-resolution capabilities. As such, in order to demonstrate the key benchmark for the capability of true atomic-resolution imaging, another current map recorded on MoS_2 is shown in Figure 1F, where a cluster of multiple atomic-scale defects is imaged, in the form of missing bright spots. On the other hand, the corresponding topography map does not show the defects, proving that the averaging of interaction forces across the blunt tip−sample interface indeed precludes the imaging of atomic-scale defects in the topography channel. Taking one step further, another current map on MoS_2 is shown in Figure 1G, where we are able to demonstrate ultimate spatial resolution under ambient conditions. In particular, three types of atomic sites (see the green, purple, and pink circles in Figure 1G) with the expected periodicity of ∼3.2 Å that feature low, high, and intermediate current are simultaneously resolved. More importantly, we can clearly identify a single atomic defect in our image, manifesting as a missing "bright spot" that is indicated by the white arrow. This latter observation unequivocally proves that we are able to achieve true atomic-resolution imaging via the method of C-AFM under ambient conditions. Comparing our results to what has been achieved on MoS_2 via STM under UHV conditions, we tentatively assign the single atomic defect in our image to an S vacancy, due to the rather isolated effect it has on the local conductivity, in contrast to electronic effects extending over several nanometers expected for Mo vacancies and various dopants.[26,27]

With our method, we are also able to image defects other than single atomic vacancies on MoS_2, as summarized in Figure 2. In particular, Figure 2A shows an atomically resolved large-scale (23.75×23.75 nm^2) current image on MoS_2 that exhibits concentrated dark defects (indicated by the blue arrow) as well as diffuse, large-area bright (indicated by pink and white arrows) and dark defects (indicated by the green arrow) that extend over a few nanometers. The contrast seen in such current maps can be associated with localized variations in the density of states (DOS) and/or charged regions.[21,22,24] This image additionally demonstrates that we are routinely able to image areas of several 100 nm^2 with atomic resolution, a feat that is challenging to perform with methods such as NC-AFM. An enlargement on the type of defects indicated by the blue arrow in Figure 2A reveals multiple atomic vacancies (similar to the case in Figure 1F). Figure 2B shows an enlarged image on the diffuse defects in Figure 2A. The uninterrupted continuation of the lattice structure over these extended defects indicates that their physical origin likely lies in the subsurface region: e.g., in the form of subsurface Mo vacancies or substitutionals.[27] We also observe individual *faint* dark spots, as highlighted by the pink dashed circle in Figure 2C, in contrast to *regular* dark spots highlighted by the blue dashed circle. Due to the fact that these defects are concentrated to single atomic sites but provide a relatively weaker contrast in current, we attribute them to subsurface S vacancies,[27,28]

https://doi.org/10.1021/acsnano.2c08321
ACS Nano XXXX, XXX, XXX−XXX

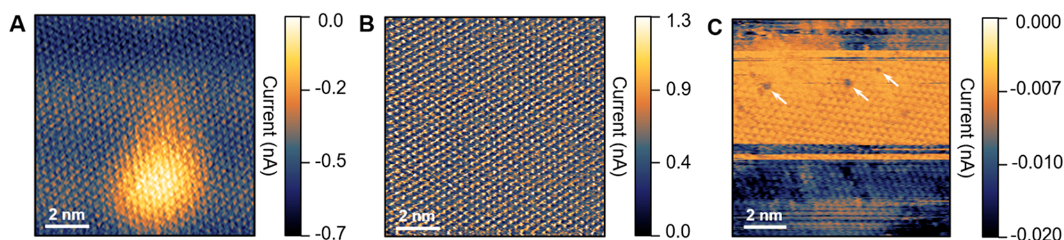

Figure 3. Atomic-resolution imaging on different material surfaces under ambient conditions via C-AFM. (A) Current image recorded on WSe_2, a 2D TMD semiconductor, showing a diffuse bright defect overlaid on a continuous atomic lattice. (B) Current image recorded on Au (111), a metal. (C) Current image recorded on $PtSe_2$, a 2D semimetal, showing several atomic-scale defects (white arrows) and frequent contrast changes. All images were obtained with an applied normal load of 0.0 nN and at a scanning frequency of 15.62 Hz. Bias voltages: (A) −1.8 V; (B) 0.01 V; (C) −0.14 V.

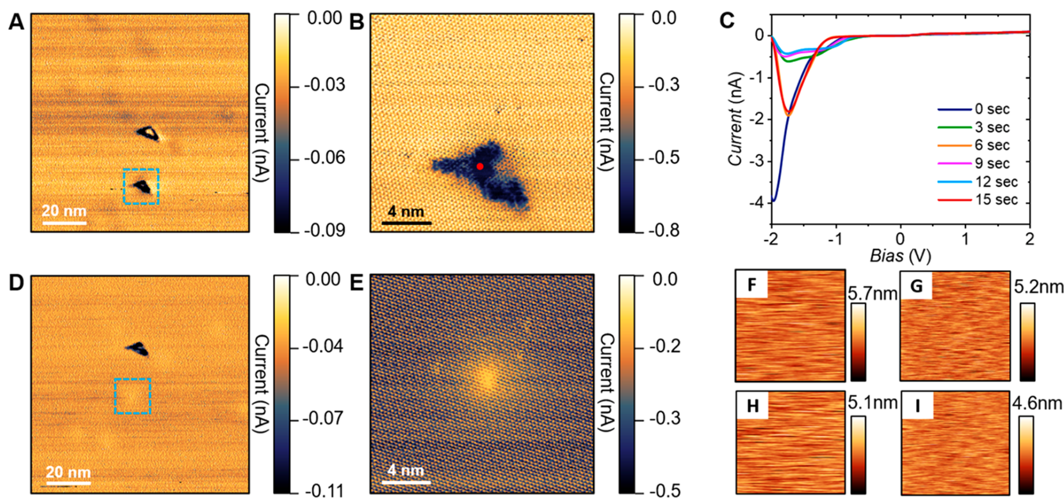

Figure 4. Electronic manipulation of a defect on MoS_2 via C-AFM under ambient conditions. (A) Large-scale current image showing two defects. (B) Enlarged current image on the defect highlighted by the blue dashed square in (A). The defect features enhanced conductivity compared to its surroundings. (C) *I*−*V* curves recorded on top of the defect location marked with the red dot in (B). (D) Current image of area (A) after the *I*−*V* sweeps. (E) Current image capturing the same defect in (B) after the *I*−*V* sweeps. The defect now features a slightly lower conductivity compared to its surroundings, with the uninterrupted atomic lattice overlaid on top of it. (F−I) Corresponding topographic images for (A), (B), (D), and (E), respectively. All images were obtained with an applied normal load of 0.0 nN and at a scanning speed 15.62 Hz. Bias voltages: (A) −1.0 V; (B) −1.3 V; (D) −0.8 V; (E) −0.8 V.

demonstrating that our approach can detect minute disturbances in the atomic structure, even below the surface. Finally, another extended type of defect is shown in Figure 2D with a lateral span of ∼6 nm. This defect features a bright region surrounded by a dark region, corresponding to enhanced and attenuated conductivities, respectively. These may be caused by local charging due to defects in the subsurface or generated during imaging due to local band bending by Coulomb repulsion.[26] It is crucial to note that all defects observed here on MoS_2 were imaged earlier with STM, under UHV conditions.[26] Our results, which provide comparable images, now prove that it is indeed possible to conduct atomic-resolution studies of defects in a 2D semiconductor such as MoS_2 simply by employing C-AFM under ambient conditions (i) without operational and instrumentational complications of STM/NC-AFM, (ii) without loss of resolution, and (iii) with the ability to decouple electronic and structural effects thanks to the separate recording of the current and topography channels.

In order to explore whether our atomic-resolution imaging capabilities are restricted to HOPG and MoS_2, we performed experiments on a number of different material surfaces, as summarized in Figure 3 (for a verification of atomic periodicities of the surfaces investigated here, please see Figure S1). In particular, Figure 3A shows a current image recorded on WSe_2 (001), exhibiting a diffuse bright defect superimposed on a continuous atomic lattice. This image proves that our methodology works on 2D TMD semiconductors other than MoS_2. Completely changing material classes, we performed C-AFM experiments on the Au (111) surface, a prototypical, close-packed metal surface of scientific importance.[29] As shown in Figure 3B, C-AFM can clearly resolve the atomic structure of the Au (111) surface, extending its realm of applicability to metals. $PtSe_2$, a semimetal and a member of group 10 TMDs,[30] was also imaged. Specifically, Figure 3C shows a current image recorded on $PtSe_2$ (001), where the atomic surface structure together with several atomic-scale defects (indicated by white arrows) can be resolved. Much like early NC-AFM images recorded on Si (111)-7 × 7,[10] this image features frequent changes in contrast that can be attributed to minute alterations in the tip apex that occur during scanning: e.g., by transfer of atoms or molecules to/from the sample surface.[31]

Going beyond imaging, we also investigated the capability of our method to electronically manipulate defects under ambient conditions. In particular, Figure 4A shows a current image of MoS_2 with two extended defects that exhibit higher conductivity than their surroundings. Magnified images on the defects allow their study with high spatial resolution

https://doi.org/10.1021/acsnano.2c08321
ACS Nano XXXX, XXX, XXX−XXX

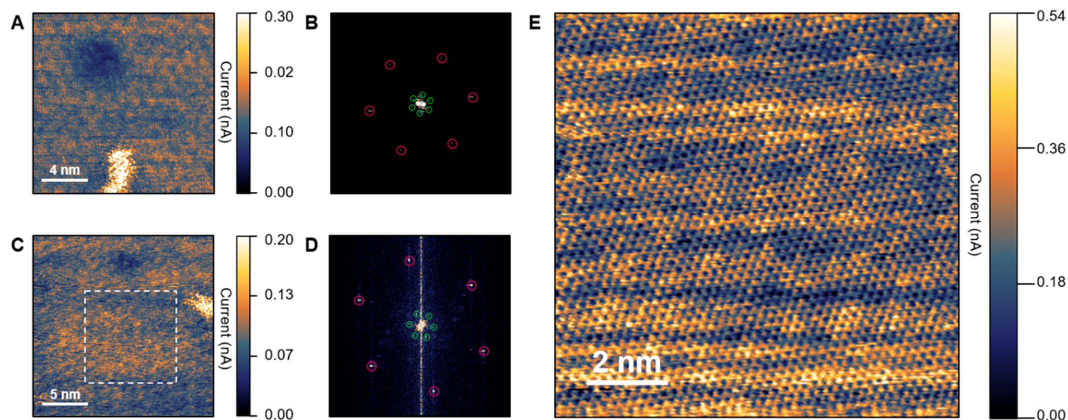

Figure 5. Observation of room-temperature charge ordering on an MXene via C-AFM. (A) Current image recorded on α-Mo_2C, an MXene, showing periodic modulation of charge, along with two defects. (B) The corresponding FT of the image shown in (A). The bright spots highlighted by red circles represent the lattice structure of α-Mo_2C with a periodicity of ~2.2 Å, while the bright spots highlighted by green circles represent the charge modulation with a periodicity of ~11.4 Å. (C) Another current image recorded on α-Mo_2C exhibiting charge ordering. (D) The corresponding FT of the image shown in (C). The bright spots highlighted by red and green circles represent lattice structure of α-Mo_2C (periodicity ~2.2 Å) and periodic modulation of charge (periodicity ~11.1 Å), respectively. (E) Enlarged current image of the area highlighted by the white dotted square in (C), showing an ordering of charge superimposed on the atomic surface lattice. All images were obtained with an applied normal load of 0.0 nN and at a scanning frequency of 15.62 Hz. Bias voltages: (A) 0.1 V; (C) 1.3 V; (E) 1.3 V.

(Figure 4B). By performing current vs voltage (I−V) sweeping for multiple cycles (Figure 4C), we found an emerging peak in the I−V curves at a bias voltage of about −1.7 V, which is first attenuated and then re-emerges during the I−V cycles. This is accompanied by a side peak appearing between −1.1 and −1.3 V. After the I−V sweeps, the high-conductivity region associated with the defect disappears (see Figure 4D,E, to be compared with Figure 4A,B). The possibility of surface contamination can be ruled out, as roughness fluctuations are not observed in the corresponding topography images (Figures 4F−I). The negative differential resistance in Figure 4C, characterized by a decrease in current with increasing voltage, may be related to localized surface charging/discharging behavior. According to the passive sign convention, more electrons may flow out of the defect location, indicating a pre-existing negatively charged region. After I−V sweeping, more positive charge will accumulate in the region to compensate the nonuniform charge states, which may explain the slightly lower current detected on the defect location after the I−V sweeps (Figure 4E). These experiments demonstrate that our method may provide a feasible strategy for localized manipulation/elimination of electrical surface defects on 2D materials under ambient conditions.

Following the demonstration of charge state manipulation of defects on MoS_2, we employed our methodology to explore exotic electronic properties of an emerging materials class. In particular, C-AFM measurements performed on thin crystals of α-Mo_2C, a prototypical member of MXenes,[32] revealed a periodic modulation (i.e., ordering) of charge, superimposed on the atomic lattice structure of α-Mo_2C (Figure 5A), in an area that includes two prominent defects. The corresponding Fourier transform (FT) shown in Figure 5B corroborates this observation, whereby the bright spots highlighted by red circles (with a periodicity of ~2.2 Å) represent the atomic structure of the α-Mo_2C surface, and the bright spots highlighted by green circles represent the periodic charge modulation with a periodicity of ~11.4 Å. Even more interestingly, the FT clearly shows the broken rotational symmetry between these two periodicities with an angular difference of ~13°. These results are supported by additional measurements on the material surface that show charge ordering (Figure 5C,E), with the corresponding FT again showing two periodicities corresponding to the lattice structure (~2.2 Å) and charge modulation (~11.1 Å), respectively, with an angular difference of ~12° between the two (Figure 5D). At this point, the question arises whether the superimposed modulations observed in the current maps can be caused by moiré patterns that involve out-of-plane undulations of the material surface due to strain.[33] Unlike STM, the C-AFM method delivers two separate channels of data for the recording of topography and current, and the absence of any structural features in topography maps acquired simultaneously with the current data here (much like the topography maps presented in the insets of Figure 1D−G) allows us to unambiguously assign the observed modulations in the current images to electronic, not structural, origins. The discovery of room-temperature charge ordering in α-Mo_2C is important not only from a fundamental point of view, as such phenomena have been very rarely reported for other members of the 2D materials family,[34] but also from a technological perspective, as it may lead to the possibility of exciting electronic device applications (e.g., for current switching) for MXenes.

Despite its potential, the C-AFM technique has traditionally suffered from poor reproducibility. A key reason behind this limitation is the wear of the conducting tip coating.[35] For the current study, we explored different types of commercially available conductive tips, including PtSi, Ti/Ir, and doped-diamond-coated conductive tips. We could only achieve lattice resolution on an HOPG sample with PtSi tips (please see Figure S2A). While we were able to achieve atomic resolution with Ti/Ir tips (please see Figure S2B), the imaging was not robust. Additionally, the longevity of both of these categories of tips were poor, as metal-coated tips tend to wear/melt easily. On the other hand, results achieved with doped-diamond-coated conductive tips were highly reproducible in the sense that we could routinely image surfaces of different materials with true atomic resolution using the same tip. Similarly, scanning repeatedly over the same defect resulted in consistent

https://doi.org/10.1021/acsnano.2c08321
ACS Nano XXXX, XXX, XXX−XXX

images, with the presence of some thermal drift (please see Figure S3).

The fact that C-AFM is able to routinely achieve true atomic resolution is unexpected, mainly because imaging is performed under contact mode operation, whereby the physical area of contact between the tip and the sample consists of multiple atoms (Figure 1A). This should in principle lead to an averaging effect and the inability to resolve atomic-scale defects, as is the case for topographic imaging.[8,9] We identify two primary factors that result in true atomic-resolution imaging capabilities for C-AFM under ambient conditions: (1) an atomically sharp conductive pathway and (2) high-speed imaging. The mechanism related to the first point can be explained by acknowledging that AFM tips exposed to ambient conditions are often covered by a poorly conducting layer of atmospheric adsorbates and potentially a thin layer of oxide.[36] When the tip scans the sample surface under a light load and a bias voltage, a small portion of the poorly conducting layer may break down, resulting in a very small, electrically conductive area (i.e., a very sharp electrical probe) that is able to distinguish between individual atoms even though a much larger portion of the tip is in physical contact with the sample (as shown in Figure 1A).[37] Alternatively, one of the "nanoasperities" potentially present on the blunt apexes of our diamond-coated tips can act as an atomically sharp conductive tip.[38,39]

By performing experiments with a wide range of imaging parameters, we determined that scanning speed plays a crucial role in achieving atomic resolution. In particular, Figures S4 and S5 showcase the effects of different scanning speeds on C-AFM imaging under ambient conditions. Specifically, as one can see in Figure S4, the spatial resolution gradually degrades with decreasing scanning speed. Conversely, Figure S5 shows that the resolution improves when the scanning speed is ramped up, showing that the observed trends are not due to irreversible modifications of the structure and/or chemistry of the tip apex during imaging. In contrast to scanning speed, the applied normal load did not seem to have an appreciable effect on imaging quality (Figure S6).

The observation that we can only achieve true atomic resolution at high scanning speeds (corresponding to ~100 nm/s and higher) points to a temporal mechanism that plays a key role in maintaining the atomic sharpness of the electrical contact. Specifically, the time spent by the AFM tip on a particular location on the sample during high-speed scanning is typically below 1 ms, which is in the relevant regime for atomic-scale aging processes at nanoscale contacts.[40] A similar argument can be made for the formation of substantial water menisci at the tip−sample contact.[41] By fast scanning, substantial bluntening of the tip−sample contact via aging effects is prevented, thus resulting in true atomic-resolution capabilities for C-AFM under ambient conditions.

CONCLUSIONS

We demonstrated that C-AFM can achieve true atomic-resolution imaging of a wide range of surfaces under ambient conditions, in a robust and reliable fashion. Going beyond imaging, we used the method to manipulate the charge state of defects in a prototypical TMD. Finally, we used our methodology to reveal an exotic electronic effect: charge ordering at room temperature on an MXene. Our approach overcomes many of the limitations associated with other SPM-based atomic-resolution imaging techniques, as it can be performed on top of a rudimentary lab bench, without the need for complicated equipment and extensive training required for UHV experiments. Perhaps more importantly, the atomic-resolution results on surface structure and properties recorded under ambient conditions will be directly relevant for technologically important applications in fields as wide as catalysis and electronics.

METHODS

Sample Preparation. ZYB-quality HOPG samples were sourced from Ted Pella and mechanically cleaved following the Scotch tape method[42] prior to C-AFM imaging. As a substrate for the TMD samples (MoS_2, WSe_2, and $PtSe_2$, all sourced from 2D Semiconductors), we used Si/SiO_2 chips coated consecutively with a ~2 nm thick adhesion layer of Ti and an ~50 nm thick Au film. TMD flakes were mechanically exfoliated on top of the Au-coated substrate via the Scotch tape method. Finally, silver paint was applied on one side, bridging the conductive specimen holder and the Au film on which the TMD flakes are located. Ultraflat Au films deposited on silicon chips sourced from Platypus Technologies were used for C-AFM imaging. Silver paint was again applied on one side to bridge the conductive specimen holder and the Au film. The α-Mo_2C samples were synthesized via chemical vapor deposition (CVD) by the group of Goknur C. Buke at the TOBB University of Economics and Technology. Details can be found in ref 43.

C-AFM Measurements. The C-AFM measurements were performed using a commercial AFM (Asylum Research, Cypher VRS) under ambient conditions (temperature, 22−23 °C; relative humidity, 20−50%). Samples were inserted inside the AFM chamber without any prior treatment for surface cleaning. Commercially available, doped-diamond-coated conductive tips (NanoSensors, CDT-CONTR, normal stiffness 0.6 ± 0.1 N/m and Adama Innovations, AD-2.8-SS, normal stiffness 1.3 ± 0.1 N/m) were used for imaging. Initially, imaging of large areas (e.g., 10 × 10 μm) was performed without any bias to find regions of interest in the sample surface. For atomic-resolution imaging, small areas such as 5 × 5 nm were scanned in contact mode with an applied bias. Imaging was usually performed under only the adhesion (i.e., *snap-in*) force acting between the tip and the sample, with no normal load applied in addition. The magnitude of the snap-in force between the tip and different samples was on the order of a few nanonewtons. A representative force−distance curve is shown in Figure S7. The bias voltage was always applied to the sample. The applied bias had to be tuned during each session, to either initiate or keep imaging the surface with atomic resolution. Potential reasons include (i) different amounts of voltages required to break down different amounts of contamination layers accumulated on different tip apexes, (ii) different electrical conductivities and tip−sample junction states for each sample, and (iii) dynamic changes occurring at the tip−sample contact during imaging in the presence of contaminant molecules under ambient conditions. An additional resistance of 10 MΩ was used in series occasionally to limit the current. The average periodicities of the atomic features observed in the images were calculated using the software Gwyddion by way of Fourier transform (FT) and line profiles.

ASSOCIATED CONTENT

Data Availability Statement

All data needed to evaluate the conclusions in this study are present in the main text or the Supporting Information. All raw data and scripts that were used for the data analysis are available from the corresponding author on request.

Supporting Information

The Supporting Information is available free of charge at https://pubs.acs.org/doi/10.1021/acsnano.2c08321.

Atomic models and experimentally recorded periodicities for different materials, images with different tip

materials, reproducibility of defect imaging, speed dependence of atomic-resolution C-AFM imaging, load dependence of atomic-resolution C-AFM imaging, and force spectroscopy (PDF)

AUTHOR INFORMATION

Corresponding Author

Mehmet Z. Baykara − *Department of Mechanical Engineering, University of California Merced, Merced, California 95343,, United States;* orcid.org/0000-0002-0278-6022; Email: mehmet.baykara@ucmerced.edu

Authors

Saima A. Sumaiya − *Department of Mechanical Engineering, University of California Merced, Merced, California 95343,, United States*

Jun Liu − *Department of Mechanical and Aerospace Engineering and RENEW (Research and Education in Energy, Environment and Water) Institute, University at Buffalo, The State University of New York, Buffalo, New York 14260, United States;* orcid.org/0000-0001-6951-8826

Complete contact information is available at: https://pubs.acs.org/10.1021/acsnano.2c08321

Author Contributions

M.Z.B. and S.A.S. conceived the experiments. S.A.S. performed the experiments. M.Z.B. and S.A.S. led the writing effort. M.Z.B., S.A.S, and J.L. participated in data analysis and the interpretation of the results.

Notes

A manuscript containing a subset of the results presented here has been previously published on the preprint server arXiv on October 5, 2021: Sumaiya, S. A.; Baykara, M. Z. True Atomic-Resolution Imaging under Ambient Conditions via Conductive Atomic Force Microscopy. 2021, 2110.01807. arXiv. https://arxiv.org/abs/2110.01807 (accessed October 6, 2022).

The authors declare no competing financial interest.

ACKNOWLEDGMENTS

This work was supported by the Air Force Office of Scientific Research (AFOSR) Award No. FA9550-19-1-0035. We thank Goknur C. Buke and her team for providing the α-Mo_2C samples.

REFERENCES

(1) Ruan, W.; Chen, Y.; Tang, S.; Hwang, J.; Tsai, H.-Z.; Lee, R. L.; Wu, M.; Ryu, H.; Kahn, S.; Liou, F.; Jia, C.; Aikawa, A.; Hwang, C.; Wang, F.; Choi, Y.; Louie, S. G.; Lee, P. A.; Shen, Z.-X; Mo, S.-K.; Crommie, M. F. Evidence for Quantum Spin Liquid Behaviour in Single-Layer 1T-$TaSe_2$ From Scanning Tunnelling Microscopy. *Nat. Phys.* **2021**, *17*, 1154−61.

(2) Peng, J.; Sokolov, S.; Hernangomez-Perez, D.; Evers, F.; Gross, L.; Lupton, J. M.; Repp, J. Atomically Resolved Single-Molecule Triplet Quenching. *Science* **2021**, *373*, 452−456.

(3) Kawai, S.; Saito, S.; Osumi, S.; Yamaguchi, S.; Foster, A. S.; Spijker, P.; Meyer, E. Atomically Controlled Substitutional Boron-Doping of Graphene Nanoribbons. *Nat. Commun.* **2015**, *6*, 1−6.

(4) Binnig, G.; Rohrer, H.; Gerber, C.; Weibel, E. Surface Studies by Scanning Tunneling Microscopy. *Phys. Rev. Lett.* **1982**, *49*, 57.

(5) Binnig, G.; Quate, C. F.; Gerber, C. Atomic Force Microscope. *Phys. Rev. Lett.* **1986**, *56*, 930.

(6) Binnig, G.; Gerber, C.; Stoll, E.; Albrecht, T. R.; Quate, C. F. Atomic Resolution with Atomic Force Microscope. *EPL* **1987**, *3*, 1281.

(7) Albrecht, T. R.; Quate, C. F. Atomic Resolution Imaging of a Nonconductor by Atomic Force Microscopy. *J. Appl. Phys.* **1987**, *62*, 2599−2602.

(8) Eaton, P.; West, P. *Atomic Force Microscopy*; Oxford University Press: 2010.

(9) Baykara, M. Z.; Schwarz, U. D. Atomic Force Microscopy: Methods and Applications. In *Encyclopedia of spectroscopy and spectrometry*; Academic Press Ltd-Elsevier Science Ltd: 2017; pp 70−75.

(10) Giessibl, F. J. Atomic Resolution of the Silicon (111) - (7 × 7) Surface by Atomic Force Microscopy. *Science* **1995**, *267*, 68−71.

(11) Ueyama, H.; Ohta, M.; Sugawara, Y.; Morita, S. Atomically Resolved InP (110) Surface Observed with Noncontact Ultrahigh Vacuum Atomic Force Microscope. *Jpn. J. Appl. Phys.* **1995**, *34*, L1086.

(12) Schimmel, T.; Fuchs, H.; Akari, S.; Dransfeld, K. Nanometer-Size Surface Modifications with Preserved Atomic Order Generated by Voltage Pulsing. *Appl. Phys. Lett.* **1991**, *58*, 1039−1041.

(13) Garcia Garcia, R. Atomic-Scale Manipulation in Air with the Scanning Tunneling Microscope. *Appl. Phys. Lett.* **1992**, *60*, 1960.

(14) Miyata, K.; Tracey, J.; Miyazawa, K.; Haapasilta, V.; Spijker, P.; Kawagoe, Y.; Foster, A. S.; Tsukamoto, K.; Fukuma, T. Dissolution Processes at Step Edges of Calcite in Water Investigated by High-Speed Frequency Modulation Atomic Force Microscopy and Simulation. *Nano Lett.* **2017**, *17*, 4083−4089.

(15) Fukuma, T.; Garcia, R. Atomic- and Molecular-Resolution Mapping of Solid-Liquid Interfaces by 3D Atomic Force Microscopy. *ACS Nano* **2018**, *12*, 11785−11797.

(16) Wastl, D. S.; Judmann, M.; Weymouth, A. J.; Giessibl, F. J. Atomic Resolution of Calcium and Oxygen Sub Lattices of Calcite in Ambient Conditions by Atomic Force Microscopy Using qPlus Sensors with Sapphire Tips. *ACS Nano* **2015**, *9*, 3858−3865.

(17) Weymouth, A. J.; Wastl, D.; Giessibl, F. J. Advances in AFM: Seeing Atoms in Ambient Conditions. *e-J. Surf. Sci. Nanotechnol.* **2018**, *16*, 351−355.

(18) Ibach, H. Adsorbate-Induced Surface Stress. *J. Vac. Sci. Technol. A* **1994**, *12*, 2240−2245.

(19) Wehling, T. O.; Novoselov, K. S.; Morozov, S. V.; Vdovin, E. E.; Katsnelson, M. I.; Geim, A. K.; Lichtenstein, A. I. Molecular Doping of Graphene. *Nano Lett.* **2008**, *8*, 173−177.

(20) Imbihl, R.; Behm, R. J.; Schlögl, R. Bridging the Pressure and Material Gap in Heterogeneous Catalysis. *Phys. Chem. Chem. Phys.* **2007**, *9*, 3459.

(21) Bampoulis, P.; Sotthewes, K.; Siekman, M. H.; Zandvliet, H. J. W. Local Conduction in $Mo_XW_{1-X}Se_2$: The Role of Stacking Faults, Defects, and Alloying. *ACS Appl. Mater. Interfaces* **2018**, *10*, 13218−13225.

(22) Nowakowski, K.; Zandvliet, H. J. W.; Bampoulis, P. Barrier Inhomogeneities in Atomic Contacts on WS_2. *Nano Lett.* **2019**, *19*, 1190−1196.

(23) Enachescu, M.; Schleef, D.; Ogletree, D. F.; Salmeron, M. Integration of Point-Contact Microscopy and Atomic-Force Microscopy: Application to Characterization of Graphite/Pt(111). *Phys. Rev. B* **1999**, *60*, 16913.

(24) Rodenbücher, C.; Bihlmayer, G.; Speier, W.; Kubacki, J.; Wojtyniak, M.; Rogala, M.; Wrana, D.; Krok, F.; Szot, K. Local Surface Conductivity of Transition Metal Oxides Mapped with True Atomic Resolution. *Nanoscale* **2018**, *10*, 11498−11505.

(25) Desai, S. B.; Madhvapathy, S. R.; Sachid, A. B.; Llinas, J. P.; Wang, Q.; Ahn, G. H.; Pitner, G.; Kim, M. J.; Bokor, J.; Hu, C.; et al. MoS_2 Transistors with 1-Nanometer Gate Lengths. *Science* **2016**, *354*, 99−102.

(26) Addou, R.; Colombo, L.; Wallace, R. M. Surface Defects on Natural MoS_2. *ACS Appl. Mater. Interfaces* **2015**, *7*, 11921−11929.

(27) Bampoulis, P.; van Bremen, R.; Yao, Q.; Poelsema, B.; Zandvliet, H. J. W.; Sotthewes, K. Defect Dominated Charge Transport and Fermi Level Pinning in MoS_2/Metal Contacts. *ACS Appl. Mater. Interfaces* **2017**, *9*, 19278−19286.

https://doi.org/10.1021/acsnano.2c08321
ACS Nano XXXX, XXX, XXX−XXX

(28) Yankowitz, M.; McKenzie, D.; LeRoy, B. J. Local Spectroscopic Characterization of Spin and Layer Polarization in WSe_2. *Phys. Rev. Lett.* **2015**, *115*, 136803.
(29) Meyer, R.; Shaikhutdinov, S. K.; Freund, H.-J. Surface Chemistry of Catalysis by Gold. *Gold Bull.* **2004**, *37*, 72.
(30) Pi, L.; Li, L.; Liu, K.; Zhang, Q.; Li, H.; Zhai, T. Recent Progress on 2D Noble-Transition-Metal Dichalcogenides. *Adv. Funct. Mater.* **2019**, *29*, 1904932.
(31) Baykara, M. Z. Noncontact Atomic Force Microscopy for Atomic-Scale Characterization of Material Surfaces. In *Surface Science Tools for Nanomaterials Characterization*; Springer: 2015; pp 273−316.
(32) VahidMohammadi, A.; Rosen, J.; Gogotsi, Y. The World of Two-Dimensional Carbides and Nitrides (MXenes). *Science* **2021**, *372*, No. eabf1581.
(33) Zhang, Z.; Gedeon, H.; Cheng, Z.; Xu, C.; Shao, Z.; Sun, H.; Li, S.; Cao, Y.; Zhang, X.; Bian, Q.; Liu, L.; Liu, Z.; Cheng, H.-M.; Ren, W.; Pan, M. Layer-Stacking, Defects, and Robust Superconductivity on the Mo-Terminated Surface of Ultrathin Mo_2C Flakes Grown by CVD. *Nano Lett.* **2019**, *19*, 3327−3335.
(34) Liu, G.; Debnath, B.; Pope, T. R.; Salguero, T. T.; Lake, R. K.; Balandin, A. A. A Charge Density-Wave Oscillator Based on an Integrated Tantalum Disulfide-Boron Nitride-Graphene Device Operating at Room Temperature. *Nat. Nanotechnol.* **2016**, *11*, 845−850.
(35) Sumaiya, S. A.; Martini, A.; Baykara, M. Z. Improving the Reliability of Conductive Atomic Force Microscopy-Based Electrical Contact Resistance Measurements. *Nano Express.* **2020**, *1*, 030023.
(36) Lantz, M. A.; O'Shea, S. J.; Welland, M. E. Characterization of Tips for Conducting Atomic Force Microscopy in Ultrahigh Vacuum. *Rev. Sci. Instrum.* **1998**, *69*, 1757−1764.
(37) Celano, U.; Hantschel, T.; Giammaria, G.; Chintala, R. C.; Conard, T.; Bender, H.; Vandervorst, W. Evaluation of the Electrical Contact Area in Contact-Mode Scanning Probe Microscopy. *J. Appl. Phys.* **2015**, *117*, 214305.
(38) Watkins, M.; Berkowitz, M. L.; Shluger, A. L. Role of Water in Atomic Resolution AFM in Solutions. *Phys. Chem. Chem. Phys.* **2011**, *13*, 12584−12594.
(39) Hiasa, T.; Kimura, K.; Onishi, H. Minitips in Frequency-Modulation Atomic Force Microscopy at Liquid-Solid Interfaces. *Jpn. J. Appl. Phys.* **2012**, *51*, 025703.
(40) Tian, K.; Li, Z.; Liu, Y.; Gosvami, N. N.; Goldsby, D. L.; Szlufarska, I.; Carpick, R. W. Linear Aging Behavior at Short Timescales in Nanoscale Contacts. *Phys. Rev. Lett.* **2020**, *124*, 026801.
(41) Riedo, E.; Lèvy, F.; Brune, H. Kinetics of Capillary Condensation in Nanoscopic Sliding Friction. *Phys. Rev. Lett.* **2002**, *88*, 185505.
(42) Novoselov, K. S.; Geim, A. K.; Morozov, S. V.; Jiang, D.; Zhang, Y.; Dubonos, S. V.; Grigorieva, I. V.; Firsov, A. A. Electric Field Effect in Atomically Thin Carbon Films. *Science* **2004**, *306*, 666−669.
(43) Turker, F.; Caylan, O. R.; Mehmood, N.; Kasirga, T. S.; Sevik, C.; Buke, G. C. CVD Synthesis and Characterization of Thin Mo_2C Crystals. *J. Am. Ceram. Soc.* **2020**, *103*, 5586−5593.

https://doi.org/10.1021/acsnano.2c08321
ACS Nano XXXX, XXX, XXX−XXX